Design of a Tsunami Warning system using Electron count data from small satellite

Team Pratham, IIT Bombay Student Satellite Program
Indian Institute of Technology Bombay, Mumbai 400076, India
manvi.dhawan@iitb.ac.in, s.shantanu@iitb.ac.in,
tusharj.iitb@gmail.com

1. Background

One of the worst disasters in last 40 years took place on December 26, 2004. Sumatra Tsunami, result of the oceanic earthquake of 9.3 magnitudes on Richter scale near Indonesian island killed over 200,000 people. The waves not only swept people away, but also destroyed well-built structures. It created a deadly series of tsunamis that swept Indonesia, India, Madagascar, and Ethiopia.

Tsunami is a series of water waves caused by the displacement of a large volume of a body of water, generally an ocean, lake due to earthquakes, volcanic eruptions and other underwater explosions, landslides. Earthquake is the mostly responsible for the major Tsunamis in ocean. The vibrations travel through the water traveling sometimes thousands of kilometers. If you were on the water or deep sea diving in SCUBA gear, you would not notice much probably just rough waves or a momentarily strong downward pull if you were underwater. However, a tsunami gains its true destructive power as it approaches land. The water level becomes shallower causing the waves caused by the earthquake to compress and combine. This is what creates the massive and destructive waves that cause so much destruction.

But the prior information of Tsunami might have reduced the devastating effect of this natural calamity at least in terms of lives.

2. Current technologies

Since Sumatra Tsunami, a large amount of research is going on to predict Tsunami so that coastal people can get prior warning. Some of these technologies are listed here:

2.1 Seismic Instruments:

In the aftermath of the Sumatra tsunami, an important effort is underway to interconnect seismic networks and to provide early alarms quantifying the level of tsunami risk within 15 minutes of an earthquake. However, the seismic estimation process cannot quantify the exact amplitude of a tsunami, and so the second step, that of tsunami confirmation, is still a challenge. The earthquake fault mechanism at the epicenter cannot exactly explain the initiation of a tsunami as it is only approximated by the estimated seismic source. The fault slip is not transmitted linearly at the ocean bottom due to various factors including the effect of the bathymetry, the fault depth, and the local lithospheric properties as well as possible submarine landslides associated with the earthquake.

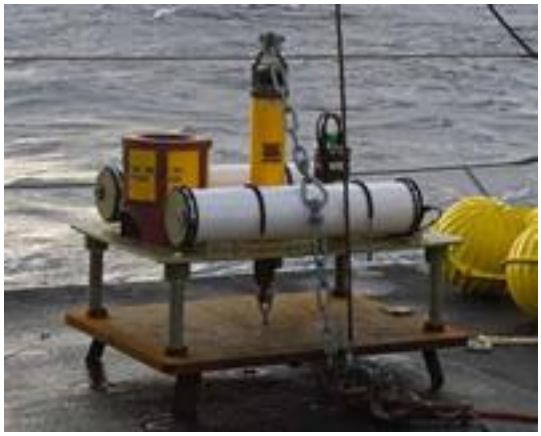

Figure 1: Pressure sensor to be deployed at ocean bed

2.2 Tide Gauges and Ocean Buoys:

The number of offshore instruments capable of tsunami measurements, such as tide gauges and buoys, is very limited. For example, there are only about 70 buoys in the whole world. As a tsunami propagates with a typical speed of 600–700 kilometers per hour, a 15-minutes confirmation system would require a worldwide buoy network with 150 kilometer spacing. In many cases, the tsunami can only be identified several hours after the seismic event due to the poor distribution of sensors. This delay is necessary for the tsunami to reach the buoys and for the signal be recorded for a minimum of one wave period (a typical tsunami wave period is between 10 and 40 minutes) to be adequately filtered by removing the “noise” due to normal wave action.

Figure 2:Tide gauge and Ocean buoy to detect Tsunami

Ocean buoys and pressure sensors at the ocean bed can be used simultaneously insync to produce more effective data as shown in figure 3.

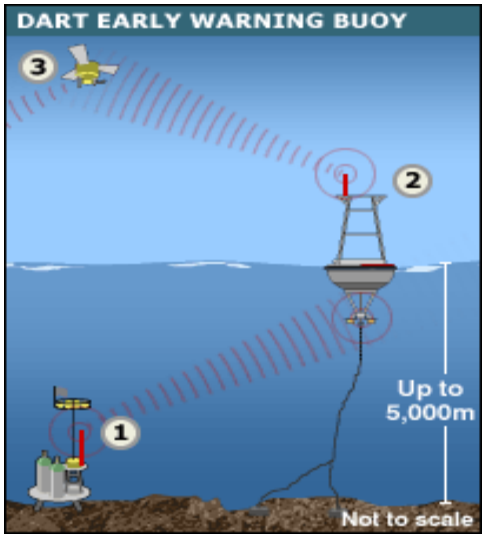

Figure 3: Recorder on sea bed measures water pressure every 15 minutes - an unusual result triggers a reading every 15 seconds. Buoy measures surface conditions and sends this plus data from sea bed to satellite which relays it to ground stations

2.3 Satellite altimetry:

Satellite altimetry has recently proved capable of measuring the sea surface variation in the case of large tsunamis, including the December 2004 Sumatra event. However, satellites only supply a few snapshots along the sub-satellite tracks. Optical imaging of

the shore has successfully measured the wave arrival at the coastline (see photo), but it is ineffective in the open sea.

Figure 4: Satellite image of Sumatra Tsunami of 26th December 2004

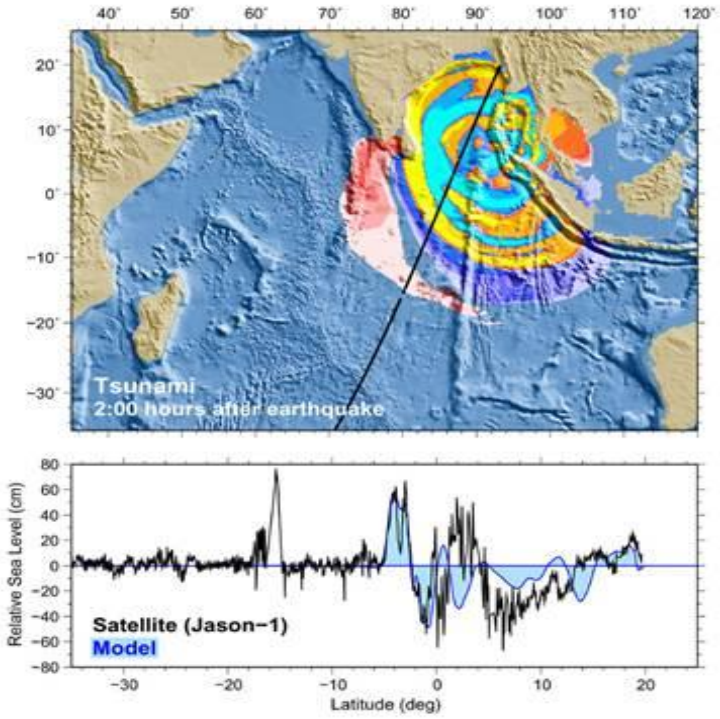

Figure 5: Satellite altimetry of Indian ocean Tsunami, 2 hours after earthquake

Ionospheric perturbations (fluctuations in Total electron count (TEC)) generated by Tsunami significantly changes the GPS readings. Measurement and monitoring of these fluctuations has the potential to provide effective Tsunami warning.

3. Ionospheric perturbations (TEC) for Tsunami detection

3.1 Total Electron Count (TEC)

TEC is the Total Electron Count of the Ionosphere. It refers to the total number of electrons in a cylinder of unit area of cross section extending from the ground station up to our satellite in space. TEC values are one of the most prominent sources of information for understanding the structure and dynamic behavior of the ionosphere. One TEC unit or TECU is 10^{16}electronsper meter-squared, equivalent to 0.162 meters of range delay at the GPS L1 frequency.

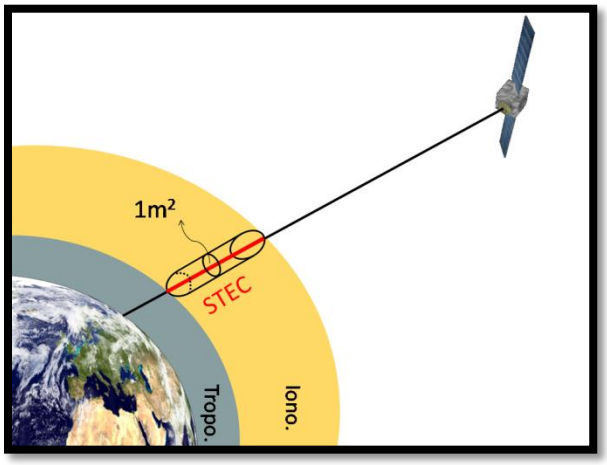

Figure 6: Total Electron Count measurement

3.2 Effect on ionospheric perturbations due to Tsunami

Recently, observational and modeling results have confirmed the existence and detectability of a tsunami-genic signature in the ionosphere. Physically, the displacement induced by tsunamis at the sea surface is transmitted into the atmosphere where it produces internal gravity waves (IGWs) propagating upward. (When a fluid or gas parcel is displaced at an interface, or internally, to a region with a different density, gravity restores the parcel toward equilibrium resulting in an oscillation about the equilibrium state, hence the term gravity wave.) The normal ocean surface variability

has a typical high frequency (compared to tsunami waves) and does not transfer detectable energy into the atmosphere. In other words, the Earth's atmosphere behaves as an "analog low-pass filter." Only a tsunami produces propagating waves in the atmosphere. During the upward propagation, these waves are strongly amplified by the double effects of the conservation of kinetic energy and the decrease of atmospheric density resulting in a local displacement of several tens of meters per second at 300 kilometers altitude in the atmosphere. This displacement can reach a few hundred meters per second for the largest events. At an altitude of about 300 kilometers, the neutral atmosphere is strongly coupled with the ionospheric plasma producing perturbations in the electron density.

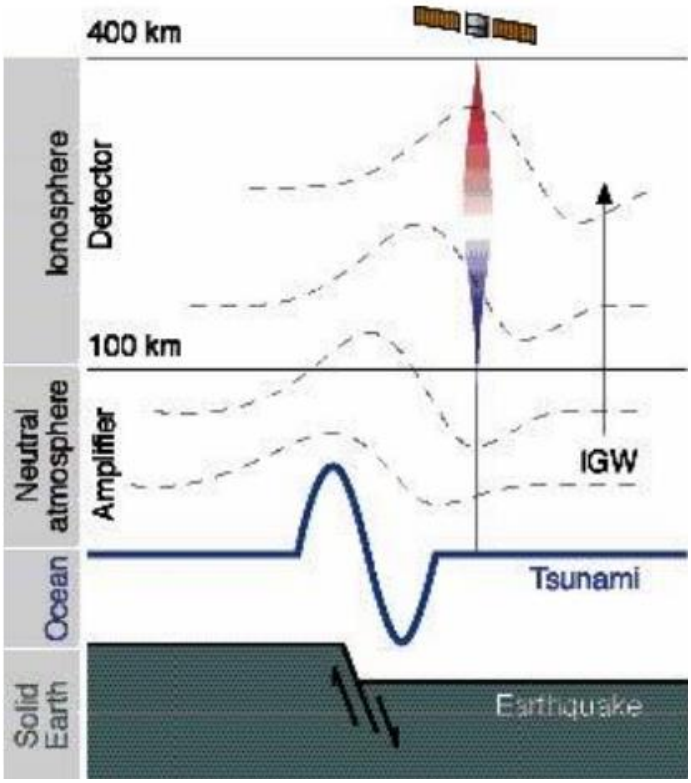

Figure 7: The tsunami-genic earthquake mechanism and transfer of energy in the neutral and ionized atmosphere

This indirect method of tsunami detection should be helpful in ocean monitoring, allowing us to follow an oceanic wave from its generation to its propagation in the open ocean. It is our hope that in the future this technique can be incorporated into a tsunami early warning system and complement the more traditional methods of detection including tide gauges and ocean buoys. Our research focuses on whether ground-based

GPS TEC measurements combined with a numerical model of the tsunami-ionosphere coupling could be used to detect tsunamis robustly. Such a detection scheme depends on how the ionospheric signature is related to the amplitude of the sea surface displacement resulting from a tsunami. In the near future, the ionospheric monitoring of TEC perturbations might become an integral part of a tsunami warning system that could potentially make it much more effective due to the significantly increased area of coverage and timeliness of confirmation.

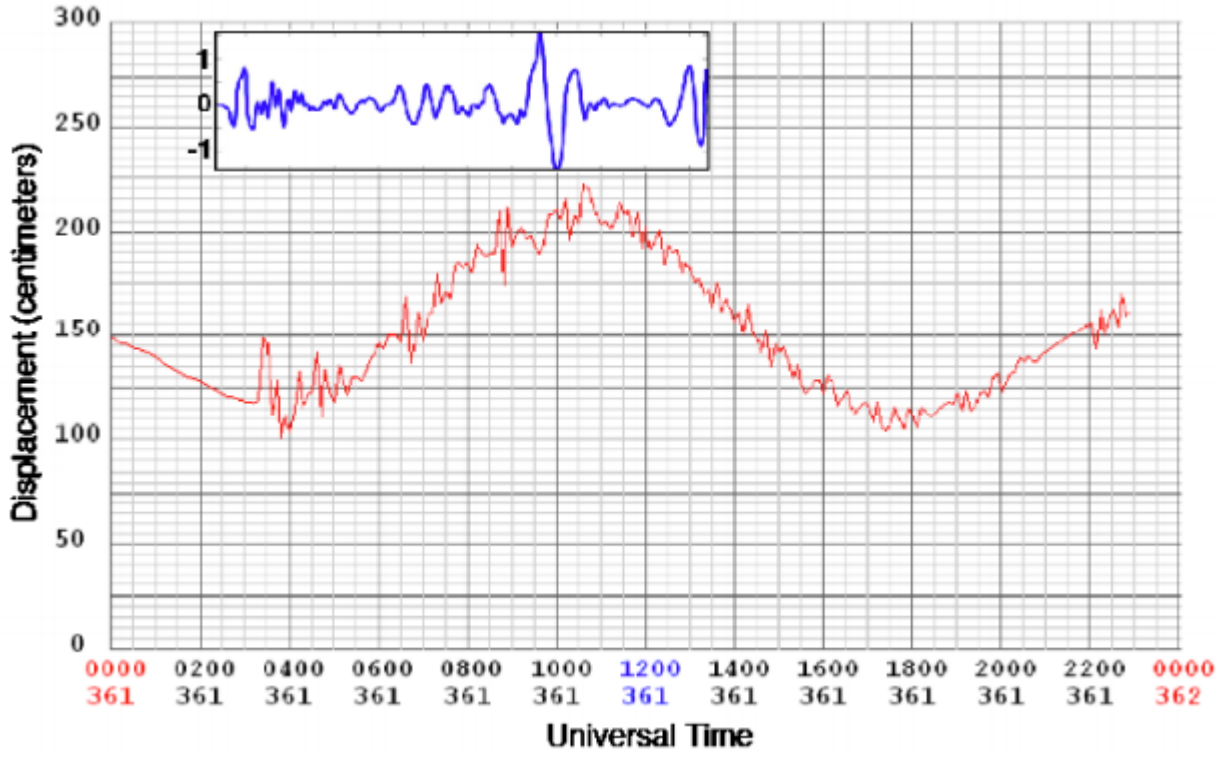

Figure 8: The Sumatra tsunami signal measured at the Cocos Islands by the tide gauge (red) and by the co-located GPS receiver (blue). The tide gauge measures the sea level displacement (tide plus superimposed tsunami) and the GPS receiver measures the total electron content perturbation (+/-1 TECu) in the ionosphere

In this article, we'll take a look at the current state of the art in modeling tsunami generated ionospheric perturbations and the status of attempts to monitor those perturbations using GPS.

3.3 Some Background

The pioneering work by the Canadian atmospheric physicist Colin Hines in the 1970s suggested that tsunami-related IGWs in the atmosphere over the oceanic regions, while

interacting with the ionospheric plasma, might produce signatures detectable by radio sounding.

The December 26, 2004, Sumatra earthquake, with a magnitude of 9.3, was an order of magnitude larger than the Peru event and was the first earthquake and tsunami of magnitude larger than 9 of the so-called "human digital era," comparable to the magnitude 9.5 Chilean earthquake of May 22, 1960.

In addition to seismic waves registered by global seismic networks, the Sumatra event produced infragravity waves (long-period wave motions with typical periods of 50 to 200 seconds) remotely observed from the island of Diego Garcia, perturbations in the magnetic field observed by the CHAMP satellite, and a series of ionospheric anomalies.

Two types of ionospheric anomaly were observed: the first type, detected worldwide in the first few hours after the earthquake, was reported from north of Sumatra, in Europe, and in Japan. They are associated with the surface seismic waves that propagate around the world after an earthquake rupture (so-called Rayleigh waves). The second type was detected above the ocean and was clearly associated with the tsunami. In the Indian Ocean, the occurrence times of TEC perturbations observed using ground-based GPS receivers and satellite altimeters were consistent with the observed tsunami propagation speed. The GPS observations from sites to the north of Sumatra show internal gravity waves most likely coupled with the tsunami or generated at the source and propagating independently in the atmosphere. The link with the tsunami is more evident in the observations elsewhere in the Indian Ocean. The TEC perturbations observed by the other ground-based GPS receivers moved horizontally with a velocity coherent with the tsunami propagation.

The amplitude of the observed TEC perturbations is strongly dependent on the filter method used. The four TECu level peak-to-peak variations in filtered GPS TEC measurements from north of Sumatra are coherent with the differential TEC at the 0.4 TECu per 30 seconds level observed in the rest of the Indian Ocean. Such magnitudes can be detected using GPS measurements since GPS phase observables are sensitive to TEC fluctuations at the 0.01 TECu level. We emphasize also the role of the elevation angle in the detection of tsunami-genic perturbations in the ionosphere. As a consequence of the integrated nature of TEC and the vertical structure of the tsunami-

genic perturbation, low-elevation angle geometry is more sensitive to the tsunami signature in the GPS data, hence it is more visible.

The TEC perturbation observed at the Cocos Islands by GPS can be compared with the co-located tide-gauge (Figure 1). The tsunami signature in the data from the two different instruments shows a similar waveform, confirming the sensitivity of the ionospheric measurement to the tsunami structure.

The link between the tsunami at sea level and the perturbation observed in the ionosphere has been demonstrated using a 3D numerical modeling based on the coupling between the ocean surface, the neutral atmosphere, and the ionosphere. The modeling reproduced the TEC data with good agreement in amplitude as well as in the waveform shape, and quantified by a cross-correlation. The resulting shift of +/-1degree showed the presence of zonal and meridional winds neglected in the modeling. The presence of the wind can, indeed, introduce a shift of 1 degree in latitude and 1.5 degrees in longitude. Since modeling is an effective method to discriminate between the tsunami signature in the ionosphere and other potential perturbations, the GPS observations can be a useful tool to develop an inexpensive tsunami detection system based on the ionospheric sounding.

3.4 Case studies

Here are some case studies which show how TECu changes due to Tsunami generation.
First case study shows the TEC contours before and after Sumatra Tsunami. The signature of the Sumatra tsunami in total electron content (TEC) at 03:18 UT (right) is compared with the unperturbed TEC (left). The TEC images have been computed by vertical integration of the perturbed and unperturbed electron density fields. The broken lines represent the Topex/Poseidon (left) and Jason-1 (right) trajectories. The blue contours represent the magnetic field inclination.

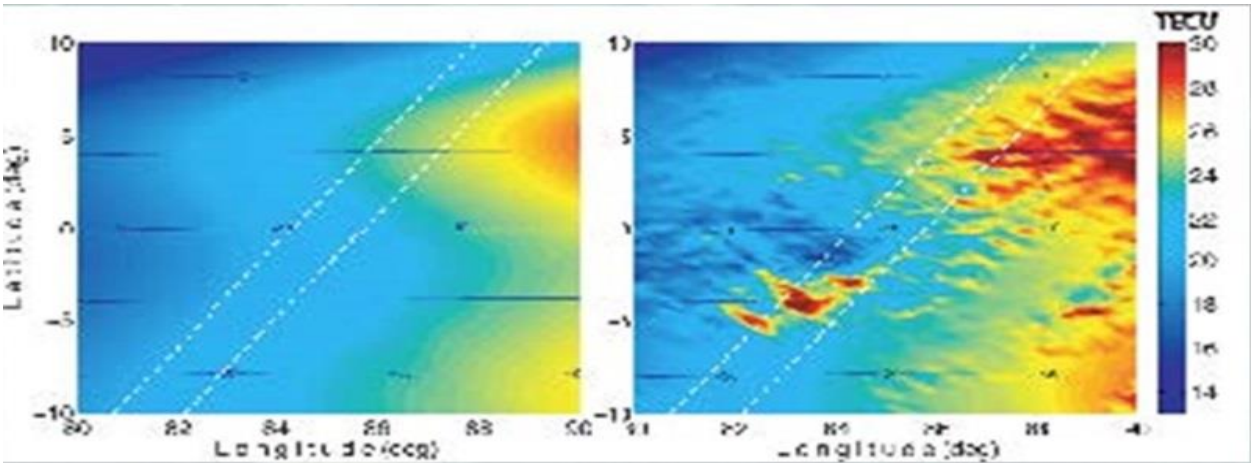

Figure 9: TEC contours before and after Sumatra (26 December 2004) earthquake [1]

A Map of the ionospheric perturbations over Japan after the Tokacho-Oki earthquake of September 25, 2003, occurring at 19h50 was created. The time interval between each map is 30s. A spectacular ionospheric perturbation is observed near the source, corresponding mainly to acoustic waves generated by the quake and appears approximately 10 minutes after. At larger distances, we also observe Rayleigh waves along the coast of the Japan Sea. The amplitudes observed are comparable to those of the Denali event and are typically 0.1 TECU peak-to-peak

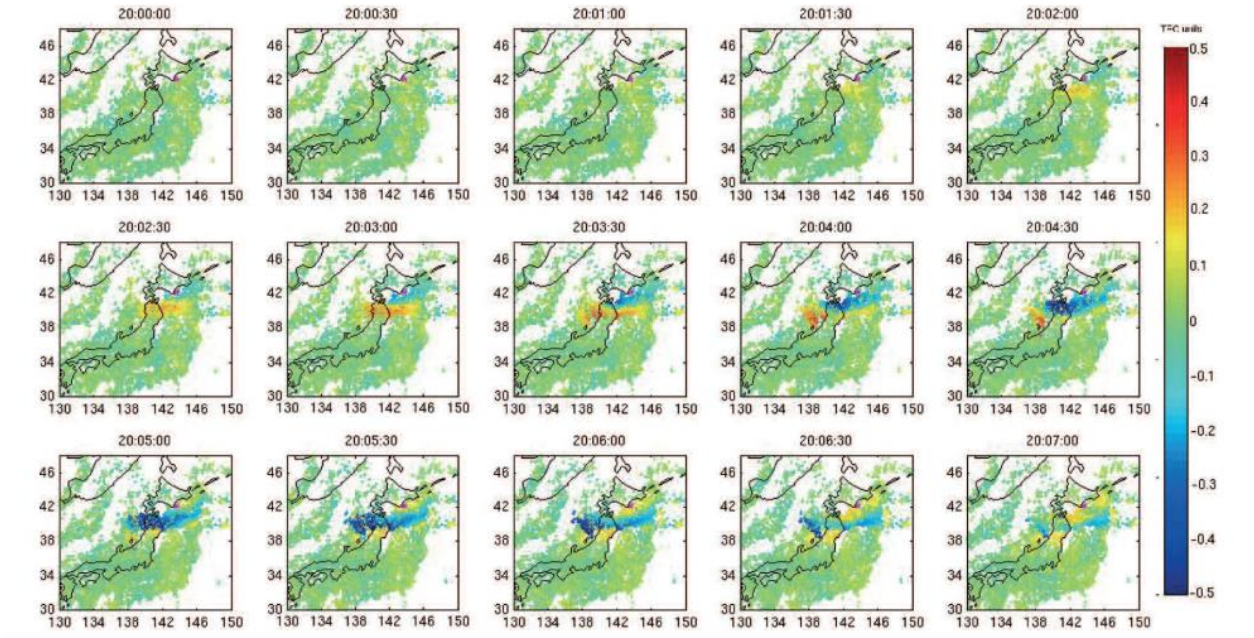

Figure 10: TEC contours before and after Tokacho-Ok (25 September 2003) earthquake. Data taken from GPS receivers on ground [2]

In June 2001, an episodic perturbation was observed following a tsunami-genic earthquake in Peru. After its propagation across the Pacific Ocean (taking about 22 hours), the tsunami reached the Japanese coast and its signature in the ionosphere was detected by the Japanese GPS dense network (GEONET). The perturbation, shown in figure (9) below, has an arrival time and characteristic period consistent with the tsunami propagation determined from independent methods. Unfortunately, similar signatures in the ionosphere are also produced by IGWs associated with traveling ionospheric disturbances (TIDs), and are commonly observed in the TEC data. However, the known azimuth, arrival time, and structure of the tsunami allows us to use this data source, even if it contains background TIDs.

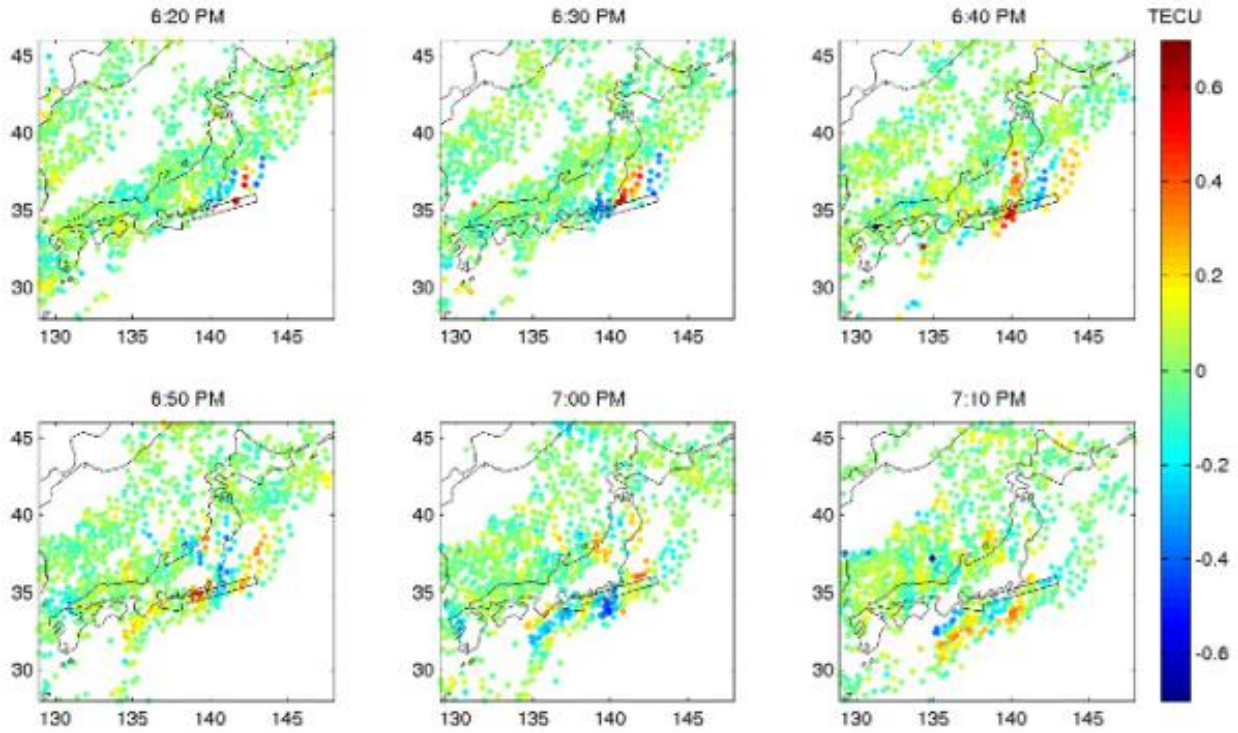

Figure 11: The observed signal for the June 23, 2001, tsunami (initiated offshore Peru) Total electron content variations are plotted at the ionosphere pierce points. A wave-like disturbance is seen propagating toward the coast of Honshu, the main island of Japan [1]

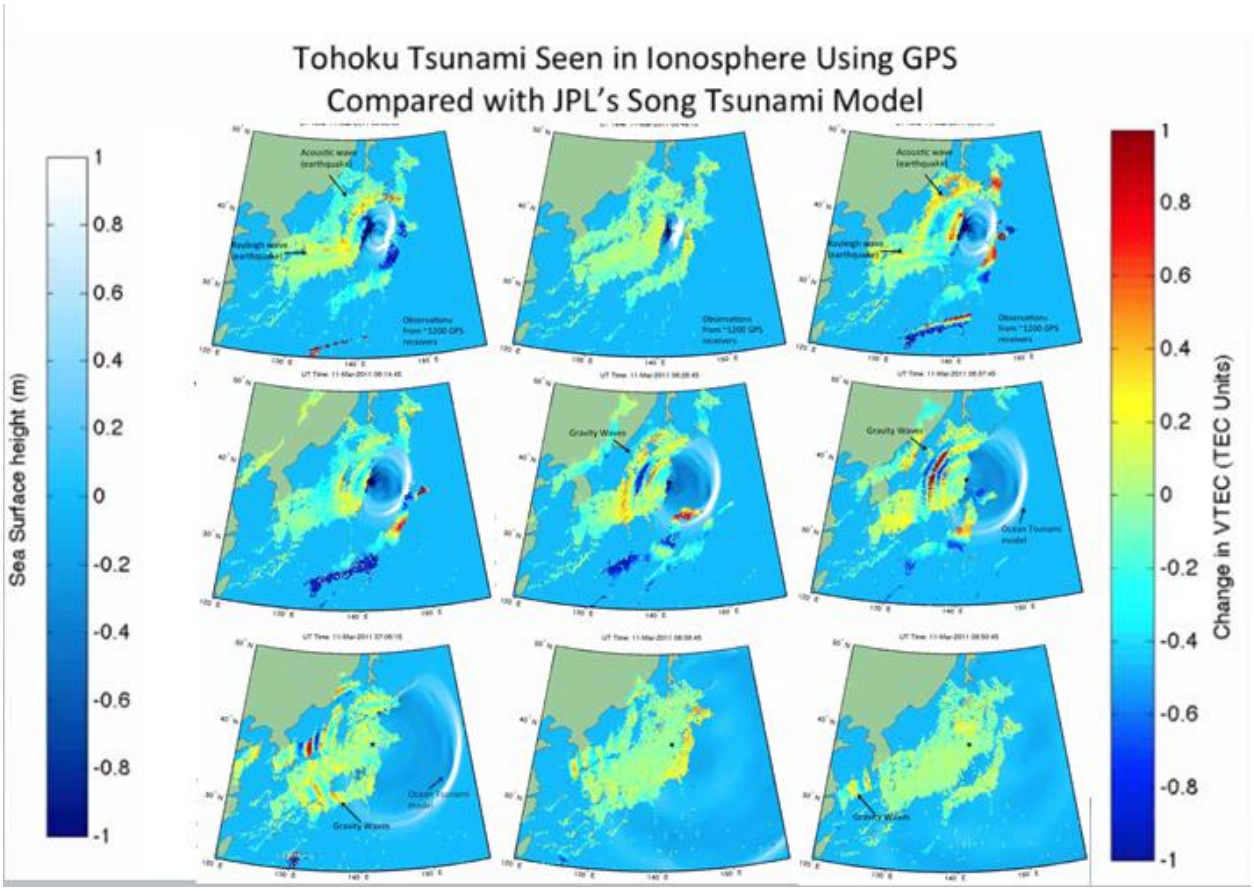

Figure 12: TEC contours before and after Tohoku (11 March 2011) earthquake. Data taken from GPS receivers on ground [4]

4. Techniques for measuring TEC from Low Earth orbit satellite

The various techniques that can be used to measure TEC from LEO satellites are described below:

- Measurement of group delay of received signal
- Measurement of Doppler shift of received signal due to ionospheric fluctuations
- Measurement of amplitude scintillations of received signal
- Measurement of Faraday rotation (our method)

4.1 Relative Group Delay of two Different Frequency Waves:

When a radio wave passes through the ionosphere, the group velocity of the wave is decreased due to the refractive index of the ionosphere. The relation between the group refractive index and the electron content of the ionosphere is given by:

$$n_g = 1 + \frac{40.3N_e}{f^2} \quad [1]$$

where N_e=electron density (in el/m^3), f=frequency of the wave (in Hz).

Now, the time delay in modulation phase is given by:

$$\Delta t = \frac{1}{c}\int_{h_1}^{h_2}(n_g - 1)dl = \frac{40.3}{cf^2}\int_{h_1}^{h_2} N_e dl \quad [2]$$

Thus this delay is directly proportional to the TEC from the satellite to the ground station. Now, suppose we send two carrier waves with the same signal upon them, the information on one will arrive faster than the other due to the $1/f^2$ dependence of this delay on the frequency. By measuring this delay between the two signals, we can detect the TEC.

Disadvantages:

- The same signal has to be imposed on two different carrier frequencies simultaneously, which is difficult
- Phase measurement at the ground station is not an easy task.

Advantages:

- The obtained reading will be directly proportional to the TEC, which is very much preferable
- There are no stringent conditions on the antennae on board the satellite

4.2 Doppler Shift due to electron density fluctuations

We know that, phase refractive index,

$$n_p = 1 - \frac{40.3N_e}{f^2} \quad [3]$$

Thus, we have that the phase of the carrier wave will depend upon the TEC as,

$$\phi = \phi_0 + \Delta\phi, \ where \ \Delta\phi = \frac{40.3}{cf}\int_{h_1}^{h_2} N_e dl \quad [4]$$

But, frequency is simply the time derivative of phase. Thus, if TEC is dependent upon time, then we will have,

$$f = \frac{d\phi}{dt} = \frac{d\phi_0}{dt} + \frac{40.3}{cf_0}\frac{d(TEC)}{dt} = f_0 + \frac{40.3}{cf_0}\frac{d(TEC)}{dt} \quad [5]$$

Thus, there will be a shift in the frequency proportional to the change in the TEC. However, this technique is useful for GEO satellites only. In case of LEO satellites the term consists of two parts:

- Due to the fast motion of the satellite relative to the ground station,
- Ionospheric fluctuations.

The typical magnitudes of the former are about 10 TECU/min whereas that of the latter is about 0.1 TECU/min. Thus, in case of LEO satellites the former factor always swamps out the latter. Thus, this method is of use only in case of GEO satellites where the former factor is absent due to the orbit of the satellite.

4.3 Amplitude and Phase Scintillations of Received Signal

The electron density of the ionosphere is not homogenous but rather it has both fine scale and large scale irregularities. These irregularities cause an EM wave to face a diffraction grating type structure of the ionosphere and as a result, when they emerge from the ionosphere, they have spatial amplitude as well as phase scintillations, just like a diffraction pattern. As the satellite passes over the ground station, these scintillations sweep over the station and as a result, we get some noisy picture. These can then be used to determine the scale of the irregularities.

4.4 Measurement of Faraday rotation of polarization angle

4.4.1 Introduction

When a linearly polarized radio wave passes through an ionized medium with a magnetic field in the direction of propagation, the plane of polarization rotates. This effect is called Faraday rotation. The relation between the rotation angle and the TEC is given by:

$$\Delta\phi = 4.87 * 10^4 f^{-2} \int_{h_1}^{h_2} NB \cos\theta \; dl \qquad [6]$$

where N = electron density, B = magnetic field of earth, θ = angle between the radio wave and line of sight, $\Delta\phi$ = angle of rotation, f = frequency of the wave

4.4.2 Measurement process:

In order to radiate linearly polarized waves from the satellite, we plan to use a monopole antenna. We will be measuring the angle of polarization at the ground station by using a crossed Yagi antenna and measuring the intensities of the signals at the two feeds. The ratio of these intensities will give us the polarization angle.

5. Ground Station Details & Data Storage

5.1 Classification of ground Stations

1) Central Ground Station – setup at IITB
2) Link Ground Station – to resolve n-pi ambiguity
3) Type I GS – Ground Station sharing the same longitude as central GS.
4) Type II GS – GS which do not share the same longitude with central GS.

5.2 Basic Functions of every Ground Station

5.2.1 Raw data Collected:

Voltage output of AD8302 which is the ratio of the signal strength from the crossed yagi's in decibels for each 145MHz and 437MHz as a function of time during the satellite pass.

5.2.2 Raw Data Processing

From the raw data the Ground Stations will generate polarization angle for 437 MHz and 145 MHz signals and the output will be written to a text file with the time of taking the reading stamped to it.

Every GS shall generate the following two kinds of information from the Polarization angle data -

1. Slant TEC tabulated against elevation angle of the satellite

a. Elevation Data:

As the micro controller stamps the voltage value measured across the AD8302, it also has to stamp the time across the voltage value. This time data stored as a vector would be input for an orbit propagator model (SGP) that outputs vector data of elevation angles corresponding to the time data. This code also requires the Two line Element of our satellite Pratham, which will be available with NORAD, Celestrack.

b. Slant TEC:

The difference in polarization angles for the 437 MHz and 150 MHz signals can be directly used to calculate TEC. This is the TEC between the satellite and the GS along the ray at the corresponding elevation angle. We call this the slant TEC (STEC). This data will be tabulated in a text file in the following format -

Name of the file has not been finalized. Tentatively : the name of the file will be stec_gs_i_yyyymmdd_hhmm.txt,
where,
“i” is the index assigned to the GS,
“yyyymmdd” is the date for the pass
and “hhmm” is the UTC in 24 hour format.

// Header data
Line 1 – Latitude of the GS
Line 2 – Number of measurements made
//Measurements made
//Elevation angle – STEC at that angle
.
.
.

2. Vertical TEC tabulated against latitude:

Vertical TEC (VTEC) at a given latitude is the TEC between the satellite and the local vertical at that latitude. VTEC is the *TEC* that is reported in the form of TEC maps.
Every GS can generate VTEC data over a certain range of latitudes about its own latitude using its own STEC measurements. This is done with the aid of what is called the *thin shell approximation*. The largest amount of electron density in the ionosphere is usually concentrated in a thin layer at an altitude of 150-200 km. Assuming the electron density were entirely concentrated in a spherical shell at an altitude of x above the earth's surface, we may write using simple trigonometry

$$VTEC_{\lambda} = (STEC_{\varphi})(\sec(\varphi+\lambda-\lambda 0)) \qquad [7]$$

where the symbols are as referenced in the figure 13. Note that corresponding to an *STEC* measurement made at some elevation angle φ , there exists some latitude λ at which the *VTEC* may be computed.
VTEC will be tabulated by every GS on similar lines as the STEC -
The name of the file will be vtec_gs_i_yyyymmdd_hhmm.txt,

where,
“i” is the index assigned to the GS,
“yyyymmdd” is the date for the pass
and “hhmm” is the UTC in 24 hour format.

// Header data
Line 1 – Latitude of the GS
Line 2 – Number of measurements made
//VTEC data
//Latitude – VTEC at latitude
.
.
.

5.3 Functions of the Central Ground Station:

The IIT-B GS will collect the STEC and VTEC files generated by every other GS' in addition to its own data regularly.

- The STEC data will be used for tomography calculations. The final product will be an ionospheric electron density plot over a latitude range covering all the GS' involved.
- The VTEC data will be compiled together and used to generate a TEC map over a latitude range covering all the GS' involved.

Finally, the following data will be made available on the Pratham website.

- TEC vs latitude maps stored as per the IONEX format in .txt files
- TEC vs latitude plots
- Electron density raw data as text files
- Electron density images

5.3.1 Ground Station Circuitry

We would be using 2 AD8302 chips (145MHz & 437MHz)to measure the relative intensities of two radio waves received by the two yagi's of the crossed yagi.AD8302 requires the signals strength given at two inputs to be greater than -60dBm & less than 0dBm. But the order of strengths received down here at the Ground Station would be

about -120dBm. So we'll be using 4 LNA's for each pin INA & INB. Two outputs of interest are VMAG & VPHS giving voltage o/p proportional to the level ratio of these signals in dB & voltage o/p between 0V – 1.8V varying linearly with phase difference between signals given at two pins INA & INB. The small signal envelope bandwidth for the two outputs is from DC upto 30MHz. If we interface the AD8302 with micro-controller of clock frequency 10KHz directly, the noise of higher frequency components (>5kHz) would decrease the SNR. So we are planning to use a low pass filter of bandwidth 5kHz in between AD8302 & microcontroller. All the cables INA, INB, VMAG, VPHS are co-axial cables.

Components of the Ground Station Circuitry:

- 2 Crossed Yagi (145 MHz & 437 MHz)
- 16 LNA's (8 for each Crossed Yagi)
- 2 AD8302 Eval Boards
- 4 Lowpass filters(band width - 5KHz)
- Micro-Controller (Clock Frequency 10KHz)

Figure 13: Ground station built at roof of Aerospace department IIT Bombay, India: 4 crossed Yagi are shown in figure out of which only two are of interest of payload

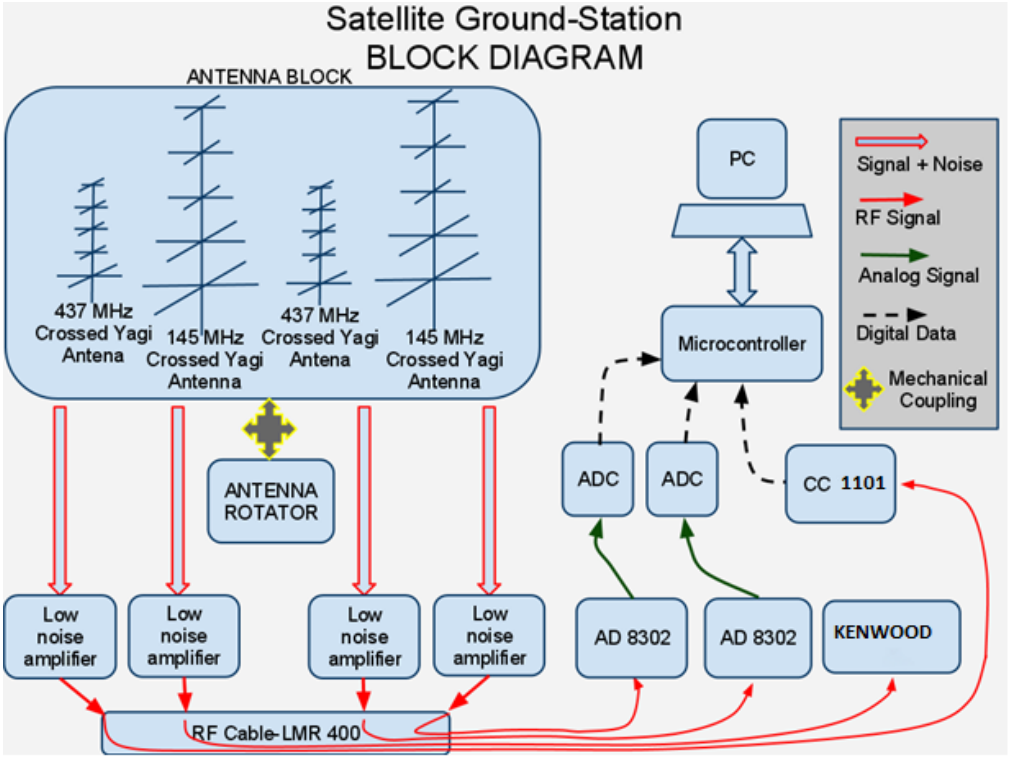

Figure 14: Satellite Ground station block diagram: Two feeds from the crossed Yagi through AD8302 are used for payload purpose. Remaining two feeds are used for telecommand and health monitoring data of satellite

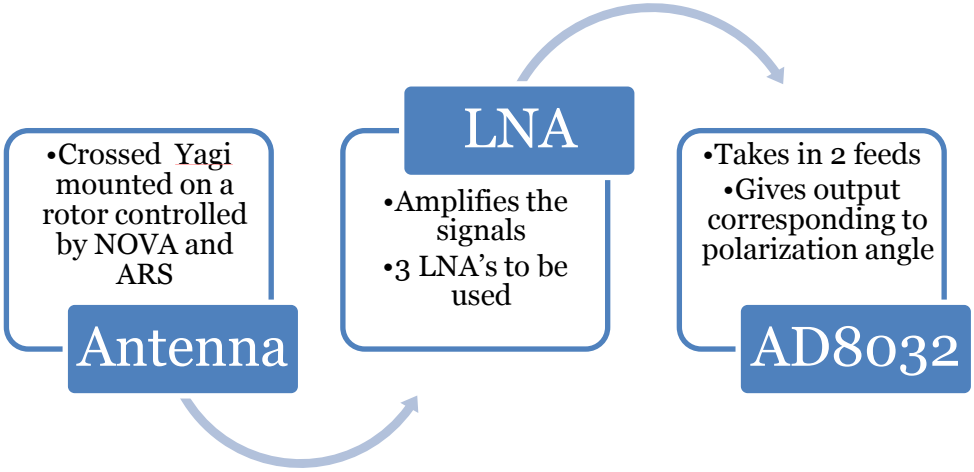

Figure 15: Flow diagram of Ground station segment used for payload

5.3.2 Measurement of phase angle by AD8302:

AD 8302 is a polarization measurement kit (phase and gain Detector) which take 2 inputs from 1 Crossed Yagi and give 2 outputs to microcontroller. We plan to measure relative intensities of the radio waves by an Analog Devices chip AD8302. This IC takes

two inputs INPA and INPB and gives a voltage o/p proportional to the level ratio of these signals in dB. In addition the pin VPHS gives the phase difference between the signals at the INPA and INPB.

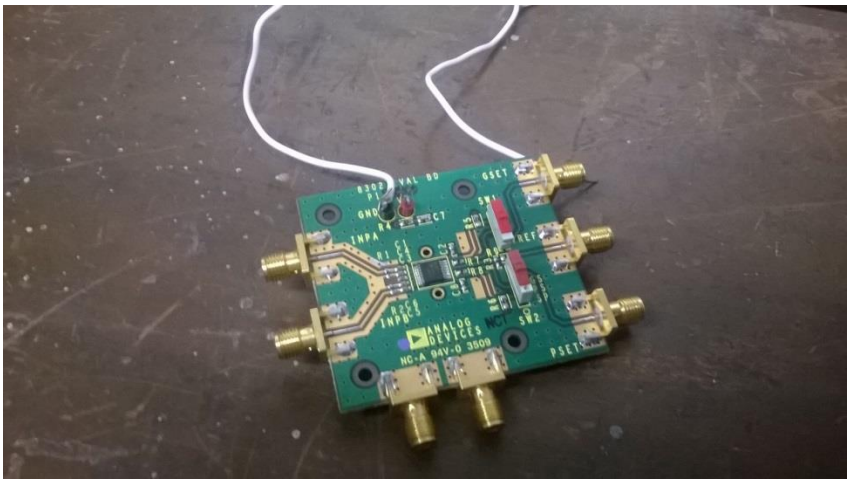

Figure 16: AD8302 Board

The output of the AD8302 is given by:

$$V = 20\, log10\, |tan\theta\,| \qquad [8]$$

where, θ is the plane of polarization

θ = tan-1 (10V/20) .....(1) OR

θ = π - tan-1 (10V/20) .....(2)

to resolve this ambiguity we need to use the phase difference information.

If the output is close to 30 mV then (1) is true.

If the output is close to 1.8 V then (2) is true.

This chip gives ±0.3 dB error for magnitude ratios within ±20 dB.

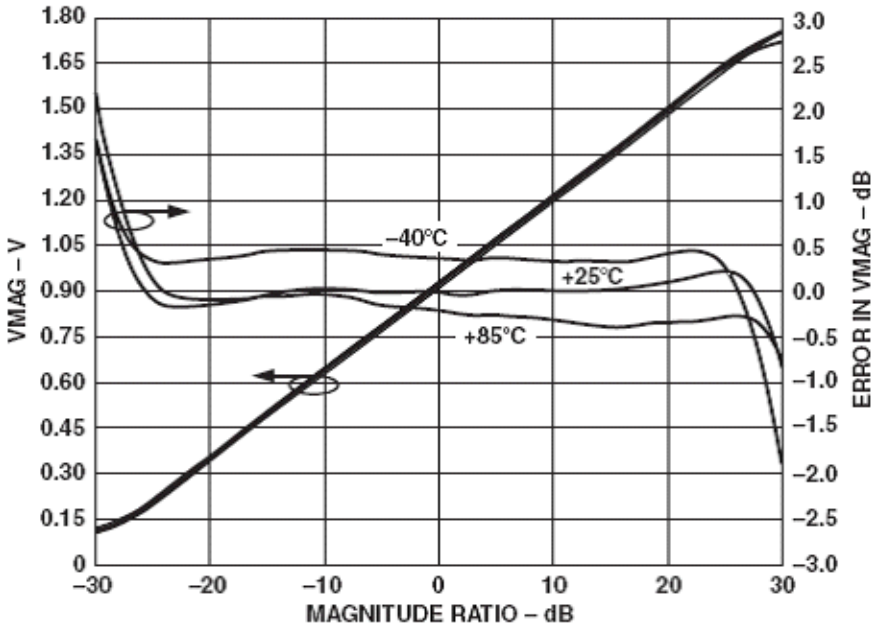

Figure 17: Voltage magnitude o/p and log conformance vs. input level ratio at frequency of 900 MHz, reference level = -30 dB

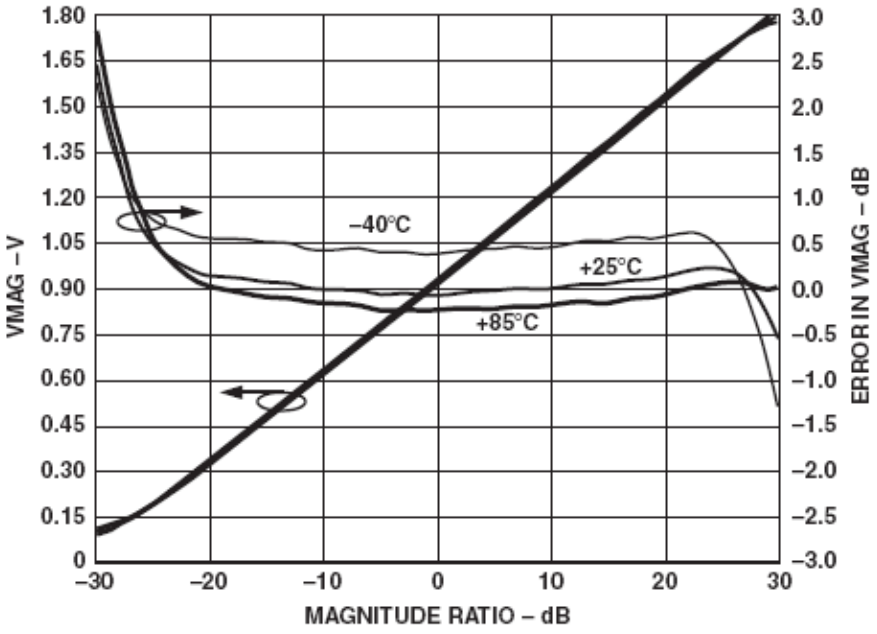

Figure 18: Voltage magnitude o/p and log conformance vs. input level ratio at frequency of 100 MHz, reference level = -30 dB

Thus, the maximum error in angle corresponding to this dB error will be ~ 1° which can give us an SNR of about 100 which will be quite good for measurements.

5.3.3 Resolution of the nπ ambiguity, use of two stations:

We will be using the two-station or the Leighteinjeir method in order to resolve the n-pi ambiguity in the measurement of the polarization angle at the ground stations. This method involves the use of readings at two ground stations simultaneously in order to determine the n-pi ambiguity at both the stations.

Here, we use the approximation that the ionospheric electron distribution is in a thin shell of uniform density. Obviously, this is a very bad approximation, but it is enough to determine the n-pi ambiguity to the nearest integer.

Under this approximation, we can write with several values of $T_{i,1}$ and $T_{j,2}$, we can fit a straight line to equation (3) for all values of i, j and we can then get least squares estimates of n1 and n2.

$$(T_{i,1} + n_1\pi)\sin\theta_{i,1} = (T_{j,2} + n_2\pi)\sin\theta_{j,2} \quad [9]$$

Where, $T_{i,1}$ and $T_{j,2}$ are the measurements taken at same locations

$\theta_{i,1}$ and $\theta_{j,2}$ are angles as shown in figure

$n_1$and n_2 are ambiguities at two stations

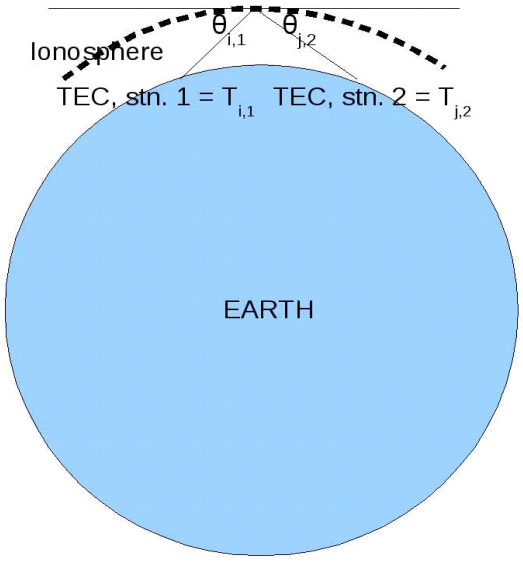

Figure 19: Leighteinjeir method

5.3.4 Simulations

Simulations of this method performed with a standard model of the ionosphere yield values of n1 and n2 which are close to the actual values. Some typical results are tabulated in the following table.

Actual value		Simulated value	
N1	N2	N1	N2
0	1	-0.19	0.87
2	2	2.18	2.08

However, measuring the angle of rotation without any attitude data on ground will be impossible as the signals will have some initial polarization angle which will depend upon the yaw of the satellite. We hence propose to use two monopole antennae operating at two different frequencies. If we keep the initial angle of polarization for the two monopoles same (by keeping their orientation), we can eliminate the effect of the initial polarization angle by taking the difference of the polarization angles measured at the two frequencies at the ground station. To achieve this, we require the yaw angle of the satellite to be 90±5 degrees and the monopoles to remain parallel within 1 degree angle. These values come from the following analysis.

5.3.5 Misalignment of antennae

The initial angle between the two waves depends upon the angle between the antennae and the position of the ground station relative to the antennae. Thus, if the two antennae are not parallel, there will be some initial angle between the waves, which we can't know unless we know the attitude of the satellite. This initial angle depends upon the yaw angle of the satellite and the elevation of the satellite above the horizon. The relation between them is brought out in the following graph.

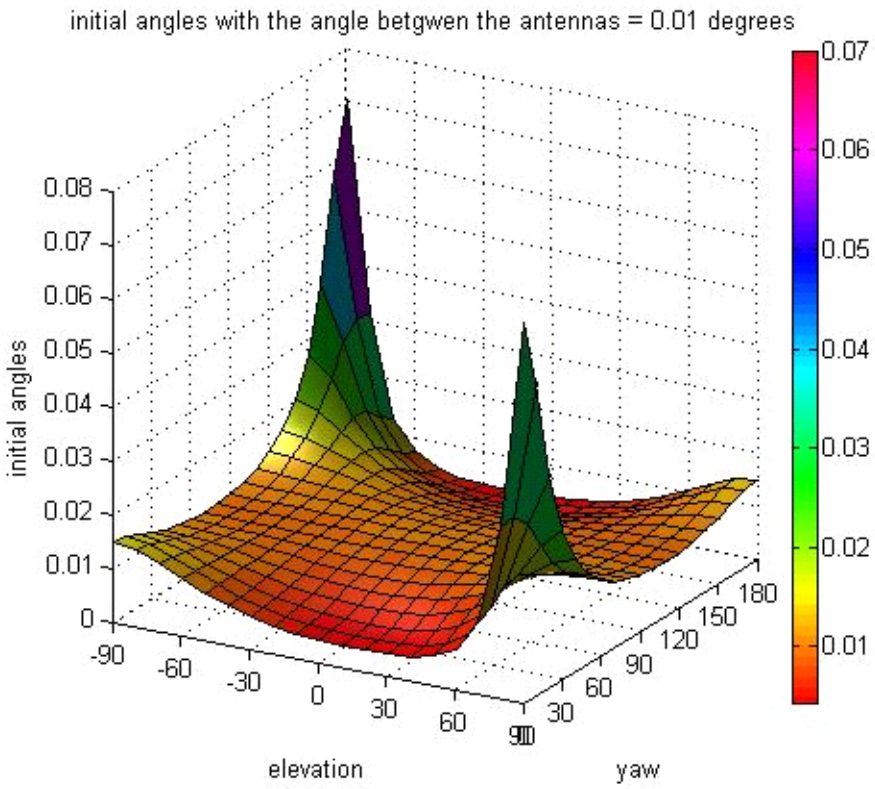

Figure 20: Misalignment of antennae

Even if we initially place the monopoles within one degree of parallelism, severe distortions can occur in the shape and position of the monopoles at the time of deployment and during launch. As we can see from the graph, the error is minimum if the satellite has a yaw angle of 90 degrees.

5.3.6 Polarization impurities and Faraday ellipticization of wave

The radio wave which will be received at the ground station will not be perfectly linearly polarized due to mainly two reasons:

Polarization impurity of the monopole antenna: The wave emitted by the monopoles aboard the satellite will not be perfectly linearly polarized because the monopoles will have a finite radius and such factors. This will introduce a circularly polarized component into the waves and thus the measurements made at the ground station will be faulty. Considering the requirement of measuring polarization angle at the ground station upto an accuracy of 1degree, we would require the monopoles on the satellite to transmit radio waves with a polarization purity of 99.9%

Faraday ellipticization of wave: When a linearly polarized EM wave passes through a medium with a transverse magnetic field and plane of polarization neither parallel nor perpendicular to the magnetic field, another effect known as Faraday ellipticization also takes place, by which the EM wave becomes elliptically polarized. However, for the frequencies we are considering, this effect will not be so important. For a frequency of 433 MHz, the minimum length needed to traverse in order to get an axial ratio of even 20dB (very weakly elliptically polarized) is of the order of 10000 km, which is far greater than what we will be experiencing (670 km).

Advantages

The advantages of Faraday Rotation technique are the following:

- Needs comparatively less hardware on board the satellite.
- Measurement is done only on carrier phase polarization angle which is an inherent property of the signal unlike a modulated signal where errors might arise.

Disadvantages

The disadvantages of this process are as follows:

- The signal transmitted from the satellite must have a high degree of polarization purity which is not so easy.
- The final result will not be directly proportional to the TEC but will depend upon the magnetic field along the path as well. Thus this dependence will have to be accounted for by some other way.
- The angle between the antennae will have to be very small.

5.4 Method and Frequencies Chosen

After analyzing all the techniques mentioned above, the Payload team decided to go ahead with Faraday Rotation for measuring the Total Electron Content of the Ionosphere. 150MHz and 437MHz were chosen as the operating frequencies since the expression for the Faraday Rotation angle clearly shows an inverse relationship with the square of the frequency. The following is a summary of the various requirements for this mission, as discussed above.

- Polarization purity of the signal from the monopoles to be better than 99.9%
- Determination of position of the satellite at the ground station up to an accuracy of 1km

- Measurement of signal strength at the ground station with an accuracy better than 0.3dB
- Maintenance of yaw angle within 90±5 degrees
- Maintenance of parallelism between the monopoles better than 1 degree

6. Ionospheric Tomography

6.1 Introduction

By Faraday rotation method, we can measure the TEC (Total Electron Content) at various elevation angles of the satellite. This gives us information about the integrals of electron density in various directions from the IIT Bombay ground station. From these integrals, we can derive the values of the electron densities at various positions of the ionosphere. This technique is called ionospheric tomography.

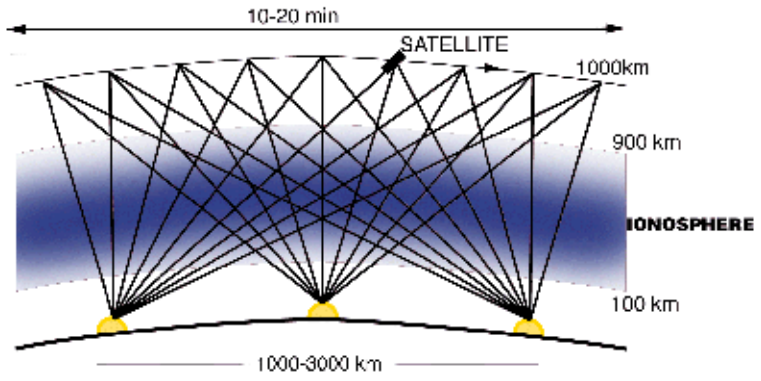

Figure 21: Geometry of the situation

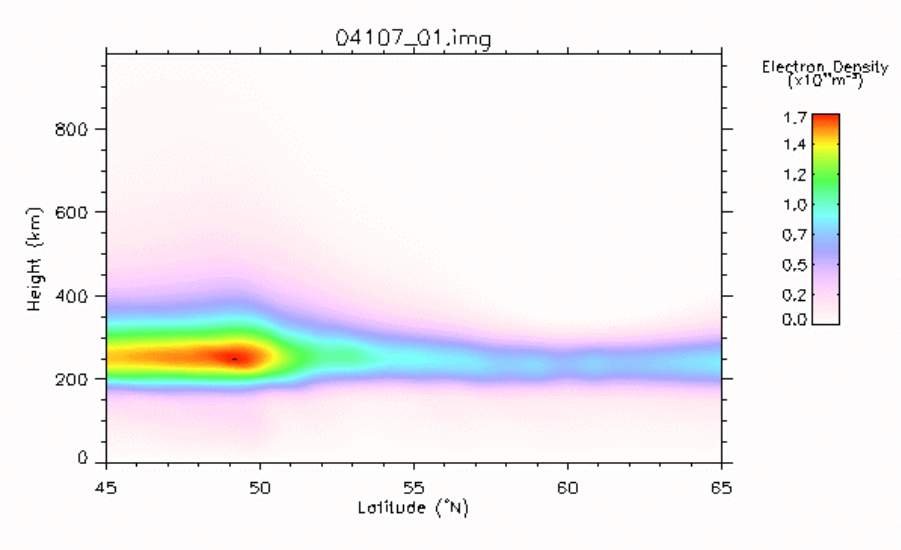

Figure 22: Tomographic image

6.2 Our technique

We will be setting up ground stations at various centers over India, preferably over the same longitude (since we wish to avoid the mixing up of temporal and spatial variations).

Algorithms:

Various algorithms are followed in tomography. These are summarized below:

Transform methods:

The procedure for these methods is:

- The derived values are transformed to a different domain (usually the frequency domain) through some transform (usually Fourier Transform).
- Then some relation between the transformed variable and the transform of the required variable is used to determine the transform of the actual variable.
- Upon applying an appropriate inverse transform, the required variable is generated.

Advantage:

Continuity of the output variable comes automatically as the inverse Fourier transform of the obtained transform is usually continuous.

Disadvantages:

- The transforms for various geometries of the measurements can lead to very different transforms for generating the required variable. This is the reason why we could not use this method in our case, as we were unable to come up with an appropriate transform for this special case
- These methods are inherently continuous. But in case of a computer, we cannot get any continuous function. Thus, there are always some discretization errors in these methods.

Algebraic methods:

The procedure for these methods is:

- The domain of the required function is divided up into pixels, i.e. discrete zones where the function is assumed to be constant.
- Then the integrals can be expressed as a linear combination of these pixel values.

- Solving these systems of linear equations, we get a solution which is a picture of the required function.

Mathematically, let the column vector consisting of the values of the electron density at various pixels be $[x_i]$. Also, let the column vector consisting of the components of the integrated electron density values at various elevation angles and at various stations be $[y_j]$. Then, the relation between [x] and [y] is given by:

$$y_i = A_{ij} x_j \qquad [10]$$

Where, A_{ij} = length of the intercept at the i^{th} pixel by the j^{th} ray

Now the problem reduces to inverting y to get x. However, the matrix A is severely rank deficient owing to the geometry of the problem and thus the problem is ill-defined. Hence we turn to the following approach to solve the problem.

We assume that an a-priori electron density vector x_o is known and use that in order to get the actual value of the electron density viz. x. This a-priori electron density can be obtained from ionospheric modeling websites. In our case, we obtained it from http://ccmc.gsfc.nasa.gov/modelweb/models/iri_vitmo.php. We seek to minimize the objective function

$$f(x) = \left|\left|Ax - y\right|\right|^2 + \alpha\left|\left|x - x_0\right|\right|^2 = \frac{1}{2}x^T(2A^TA+)$$

$$= \tfrac{1}{2}x^T(2A^TA + \alpha Ix) - (2y^TA + \alpha x_0^T x) \qquad [11]$$

Where α is a variable parameter expressing our relative confidence in the TEC data and the assumed data. We also place the constraints on x that the neighbouring pixels don't differ by too much (assumed to be greater than 2 times the corresponding difference in the base picture). This translates to

$$A_{in}x = b_{in} \qquad [12]$$

Where A_{in} and b_{in} are some matrices. Furthermore we also confine x to be within some bounds. Specifically, we say that,

$$\alpha x_{0,i} \leq x_i \leq \beta x_{0,i} \qquad [13]$$

Where α and β are some constants. Here, they are chosen to be 0.5 and 2.5 respectively.

Simulation Procedure

The simulation was carried on a part of the ionosphere above a certain longitude, spanning certain fixed ranges of latitude and altitude. This two-dimensional space is divided into a grid consisting of equally spaced radial lines, at 1° and circular arcs, at 10 km. Further, five ground stations were considered, each of which has a fixed field of view. Assuming the satellite is at a fixed orbital height, we calculate the TEC values received by the ground stations along a large number of paths. In order to do so, the length matrix is first calculated in the following manner.

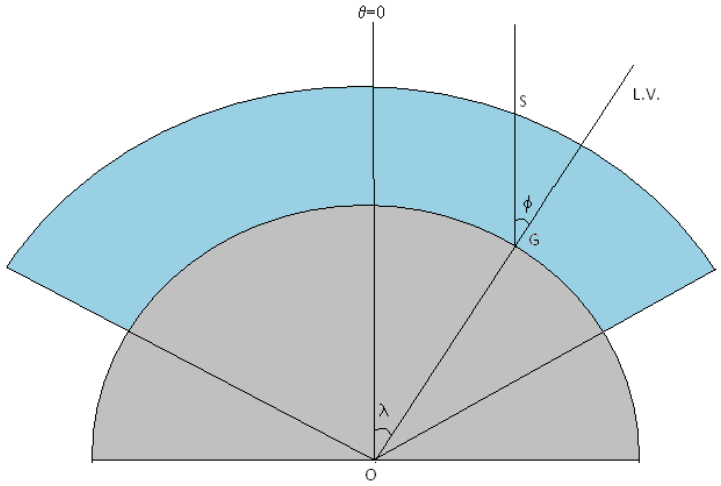

Figure 23: O – origin, G – ground station, S – satellite, L.V. – local vertical

We work in a two-dimensional polar co-ordinate system, with the centre of the earth as origin and the radial line at the equator as the pole. To obtain the $(i,j)^{th}$ entry of L, i.e. the length of the intercept made by the i^{th} ray in the j^{th} cell of the grid, we proceed as follows. The ray is represented by an equation of the form

$$r \sin\theta = mr\cos\theta + R(m\cos\lambda - \sin\lambda) \qquad [14]$$

where R = radius of the earth, λ =latitude of the ground station, m = slope of the ray = tan(ϕ), where ϕ is the angle between the ray and the local vertical. Each cell in the grid is represented by its bounding curves.

We solve the ray, with each of the bounding curves of a particular cell, and determine if the ray does intersect the cell. If so, we calculate the distance between the two points of

intersection and enter this as L(i,j). Else we enter zero. Thus the length matrix, L is constructed. We then obtain the TEC vector.

Now, this problem reduces to a quadratic programming problem, which we solve by the program ILOG CPLEX package. The results are shown below.

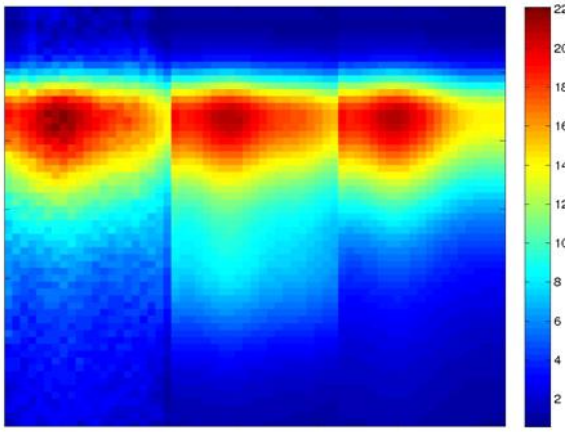

Figure 24: Assuming 5 ground stations each with 3 degrees latitude interval between them and no noise in the TEC data

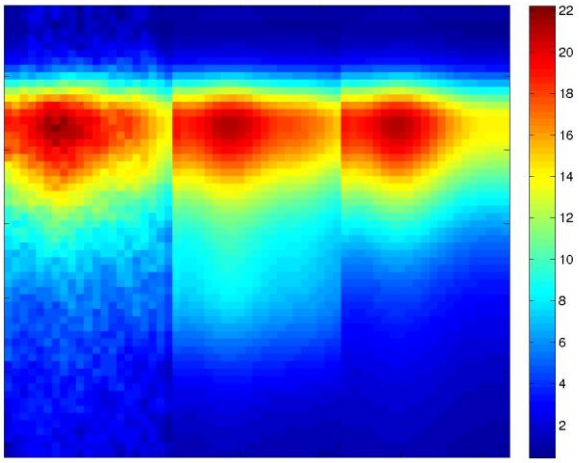

Figure 25: Assuming 2.5% normally distributed noise in the TEC data

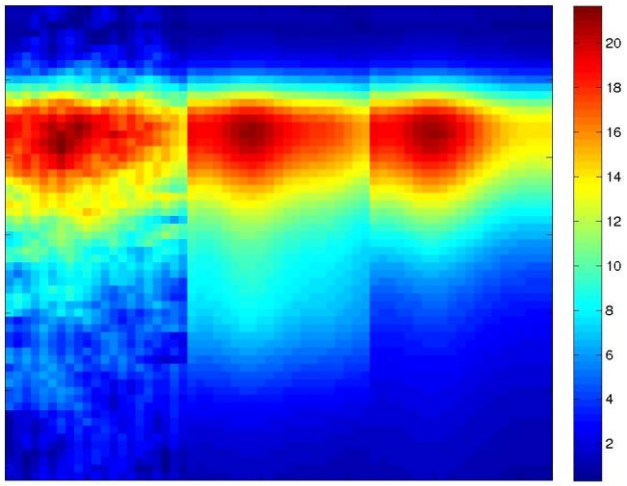

Figure 26: Assuming 10% normally distributed noise in the TEC data

In each of the above pictures, the figures in order from left are:

a) The reconstructed electron density profile

b) The actual electron density profile used to generate the TEC values

c) The base profile i.e. x_o.

We introduced an extra peak in the base value to get the actual electron density profile. It can be seen that the reconstructed profile gets worse as the noise increases.

7. Benefits of the proposed small satellites and sensors approach over existing solutions

- All the measurement and computation required for payload is done on ground. Thus no computation is required onboard for payload purpose.
- No specific hardware is required on the satellite except two monopoles each of 20.7 cm length for payload. This saves the space and power. Energy requirement of downlink monopole and circuit is 3.41 W-hr.
- After the generation of Tsunamis, it takes about 15 minutes for the IGWs to reach the ionosphere layer. Hence if a satellite and a ground station are present at appropriate location, a pre-warning can be given within 20 to 30 minutes after the earthquake. Hence the coastal areas which are at the distance more than 30 minutes from the earthquake epicenter can be effectively prevented from the adverse effects of Tsunami.

- The exact impact of Tsunami can be quantified. There are existing TEC maps which quantify the TEC variations caused due to earthquake. Hence the measured TEC map can be compared with existing contours and magnitude of Tsunamis can be estimated

8. Key Requirements on satellite and ground station position

The main requirement to detect Tsunami is to have satellite above epicenter at the time of earth quake, communicating with the ground stations. Location of the ground station should be such that the line of sight of the ground station passes through affected volume of ionosphere due to internal gravity waves. Earth quake prone area should have atleast one ground station neat by.

9. Social Goal and collaborative project development

A network of ground stations is required to collect the TEC data which would cover Tsunami prone regions. Keeping this in mind, the Pratham team had conducted a series of workshops regarding low cost ground station (Rs 50000) for various university students. Ground stations have been built at IIT Bombay, Atharva College of Engineering, Mumbai, College of Engineering, Pune (COEP), Bharati Vidyapeeth College of Engineering, Navi Mumbai, Institut de Physique du Globe de Paris (IPGP).

The IIT Bombay Student Satellite Team has founded a society named Student Satellite Society of India. Under this initiative, the team aims to bring together all the universities who have built or aim to build a student satellite. The society will give technical and non-technical support except funding to the new students who wish to enter this field. It is aimed to encourage a chain of satellites that can facilitate the transmission of two linearly polarized light waves. Since TEC payload does not require specialized hardware and power requirement is also very low, it can be accommodated in a small satellite without interfering with the existing payload. So here 2 goals can be achieved simultaneously:

1) More student satellites in India with their payload

2) More satellites to measure TEC

The proposed TEC Sensor can also be flown as an experiment on any LEO satellite to be launched by ISRO or NASA missions. Successful manifestation and implementation

of such a sensor/payload experiment will pave a cost effective to incorporate on the constellation of small satellites, or be provided as a payload to the stakeholder.

10. References

1. Giovanni Occhipinti, Attila Komjathy, & Philippe Lognonné (2008). Tsunami Detection by GPS: How Ionospheric Observations Might Improve the Global Warning System
2. Philippe Lognonné, Raphael Garcia, François Crespon, Giovanni Occhipinti , Alam Kherani and Juliette Artru-Lambin, Seismic waves in the ionosphere
3. Coïsson, P., Occhipinti, G., Lognonné, P., Molinié, J., & Rolland, L. M. (2011). Tsunami signature in the ionosphere: A simulation of OTH radar observations. *Radio Science*. doi:10.1029/2010RS004603
4. A. Komjathy, D. A. Galvan, P. Stephens, M. D. Butala, V. Akopian, B. Wilson, O. Verkhoglyadova
5. , A. J. Mannucci, and M. Hickey, Detecting ionospheric TEC perturbations caused by natural hazards using a global network of GPS receivers: The Tohoku case study. Earth Planets Space,64, 1287–1294, 2012
6. IIT Bombay, Pratham Student Satellite Project, Critical Design Report, Payload Sub-System
7. IIT Bombay, Pratham Student Satellite Project, Critical Design Report, Communication Sub-System